# Measuring nanoNewton forces with an indigenous atomic force microscope

*Achintya Singha, Anushree Roy, Anil Sonkusare, Pradeep Kumar and A. D. Kaul*

*The Atomic Force Microscope (AFM) is a versatile tool in experimental research. The principle of operation of the AFM is based on the measurement of force fields between an atomically sharp tip and surface atoms of metals or insulators. In this note, we demonstrate the ability and limitation of an indigenous AFM, designed and fabricated by us, for various measurements. In particular, short- and long-range interactions between two surfaces, of different geometrical configurations, have been measured and analysed. Our results indicate the reliability of our instrument for measuring forces in the nanonewton scale.*

The Atomic Force Microscope (AFM) is a commonly used tool in various scientific investigations, especially those which require high-resolution measurements. The AFM, also known as the Scanning Force Microscope (SFM), was invented in 1986 by Binnig, Quate and Gerber[1]. The instrument, designed by them, was a combination of a scanning tunnelling microscope[2,3] and a stylus profilometer[4]. It was shown that this type of microscope is capable of measuring interatomic forces between single atoms of metals and insulators. In the last 20 years, with added sophistication and the use of newer techniques, the range of measurements with an AFM has broadened considerably. The use of the AFM now encompasses not only the arena of basic research in science, but also industry. For example, AFM microdissection has been applied on extended chromatin fibres or single-DNA plasmid molecules to isolate the smallest cytogenetic samples[5]. In the modern nanotechnology realm, the AFM is commonly used in chip designing and fabrication[6].

The principle of operation of an AFM is shown in Figure 1. The main components of this instrument are: (i) a thin micron-sized cantilever with an extremely sharp (10–100 Å in radius) probing tip, (ii) a 3D piezo-electric scanner (piezoelectric transducer/PZT), and (iii) an optical system to measure the deflection of the cantilever. The cantilever of an AFM is of tiny dimensions: typically 100 μm long, 10 μm wide and 1 μm thick (in comparison, the average thickness of a human hair is 50 μm). At the free end of the cantilever, there is a sharp cone-shaped or pyramid-shaped tip. It has a spring constant of less than 1 nN/nm, which is orders of magnitude lower than the effective spring constant that holds the atoms (10–100 nN/nm) of the sample together. Thus, the force between the tip of the cantilever and the atoms on the surface varies, depending on the separation between the two. For 2D imaging of the surface, the sample moves in a raster scan below the sharp probe. The tip scans the profile of the surface atoms, thereby measuring the force between it and the surface at each point (Figure 2). The cantilever acts as a lever and reflects the laser beam off its tip (Figure 1). The reflected laser beam falls on a four-quadrant position-sensitive photo-detector (PSD). When the cantilever is brought close to a sample fixed on the scanner, it senses external forces and gets deflected. The reflected laser spot then strikes a new position of PSD. The difference between photodiode signals indicates the angular deflection of the cantilever. The large distance between the cantilever and the detector compared to the length of the lever can magnify the deflection of laser light from the tip of the cantilever by as much as 2000 times[7]. The detector converts this difference signal to voltage. This voltage is sensed and compared in a DC feedback amplifier circuit. The feedback circuit keeps the cantilever deflection to a pre-determined constant value by adjusting the voltage applied to the positioning PZT. As the force experienced by the cantilever is kept constant through the feedback circuit, this mode of operation is known as 'constant force' mode. When the electronic feedback circuit is switched off, the force, which causes the deflection of the tip on the sample, is directly recorded by the instrument. The microscope is said to be operating in 'constant height' mode. Even in this mode, it is preferable to keep a small amount of feedback-loop gain, to avoid the effect of thermal drift or damaging of the cantilever by a rough sample.

In the AFM, the above beam-bounce method using an optical lever, introduced by Meyer and Amer[8,9], is much less complicated than optical interferometry. Nevertheless, to measure the deflection of the cantilever, this technique achieves a resolution comparable to an interferometer. An AFM has two measures of resolution: (i) in the plane of the measurement and (ii) in the direction perpendicular to the surface. In the case of in-plane resolution, the tip of the cantilever is usually rounded-off. In addition to tip–sample interaction effects, this radius of curvature of the tip generally limits the resolution of an AFM. The in-plane resolution depends on the geometry of the probe. Commonly, the sharper the probe, the higher is the resolution of an AFM image.

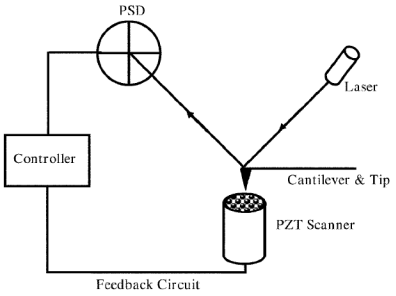


**Figure 1.** Principle of operation of an AFM (not to scale).

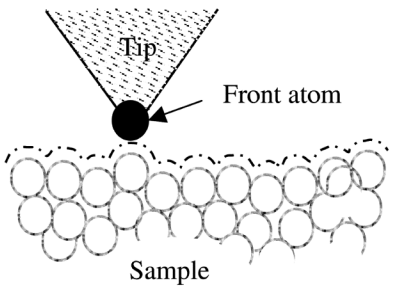


**Figure 2.** Cantilever tip following the contour of surface atoms.

Figure 3 represents a schematic diagram for the line scans of two spheres, measured with a sharp probe and a blunt probe. The vertical resolution of an AFM depends on the relative vibrations of the probe above the surface. It depends on softness of the cantilever and sensitivity of the photodetector of an AFM. Sources for vibrations, like acoustic noise, floor vibrations, thermal vibrations and electronic noise limit the vertical resolution of an AFM.

Next, we mention some common artifacts that occur in surface images, taken by an AFM, due to the behaviour of the piezo-electric scanner. (i) Nonlinearity of the image: When a linear voltage ramp is applied to the piezoelectric ceramic through the feedback circuit, the ceramic can have a nonlinear response. This causes a distortion in the image. Without nonlinearity correction, the features of an image will typically appear smaller on one side than on the other. In Figure 4 *a*(i) and (ii) we have shown schematically the distorted image of a pattern with squares and that due to nonlinearity of the piezoelectric scanner respectively, in an AFM. (ii) *Z*-edge overshoot: The hysteresis in the piezoelectric ceramic can cause edge overshoot in the perpendicular motion to the surface, i.e. in height measurement. It can be easily seen through the edge overshoot in a line profile analysis of an image. In Figure 4 *b*(ii) we have shown the overshooting of the line profile of the test pattern (Figure 4 *b*(i), at the top and at the bottom of each scan line due to hysteresis in the scanner. (iii) Drift in AFM images: The creep in the piezoelectric scanner and change in ambient temperature cause a drift in the image at the beginning of a scan. This artifact causes the initial part of a scan range to appear distorted (Figure 4 *c*). (iv) *X*–*Y* angular distortion: If the motion of the scanner in the *X* and *Y* directions is not orthogonal, an error in measurement is introduced in the 2D surface-scan. This artifact can be seen by imaging a test pattern with squares (Figure 4 *d*). The error in orthogonality can be measured using straight edge – the orthogonal red dotted lines drawn on the AFM image show that the scanner does not have a measurable crosstalk between the *X* and the *Y*-axes. (v) *Z*-angular distortion: The motion of the piezoelectric ceramic in the *X* or *Y* direction and the *Z* direction can be mechanically coupled. This causes an error in measuring side-wall angles of an angular structure with the AFM. This error can be tested with a sample of repeating triangular structures. The line profile of a symmetric triangular structure (Figure 4 *e*(i)) appears asymmetric (Figure 4 *e*(ii)) due to crosstalk between *X*/*Y* and *Z* axes of the scanner.

In the above we have discussed the basic principle of operation of an AFM, in general. However, in the literature we find different uses of this instrument with its various modifications. In India, imported AFMs are extensively used for surface imaging. We find only a few reports on design and development of indigenous AFM for this common purpose[10,11]. To the best of our knowledge, there is no report where the capability of an indigenous AFM for sub-nanonewton force field measurements has been discussed in detail. We have designed and fabricated the instrument indigenously. Next we present the details of the microscope design and then discuss the calibration of the microscope and the study of a few samples (of nanoscale dimensions) grown by us. Quantitative measurements of force between the tip and the surface under different conditions are discussed next. Finally, we discuss the capabilities and limitations of the instrument with a few concluding remarks.

## Instrumentation

As mentioned before, the operation of an AFM is based on measurement of force of the order of nanonewton. One needs precision in the designing of the instrument to measure such a tiny force. Figure 5 *a* shows a photograph of the AFM designed by us. The operation of the microscope is controlled by an electronic controller and a data-acquisition system. The electronic systems are interfaced with a computer for acquiring data, transforming the data to the display of sample images and for measuring force.

The mechanical scanning system of our AFM consists of a piezo tube (EBL#2,

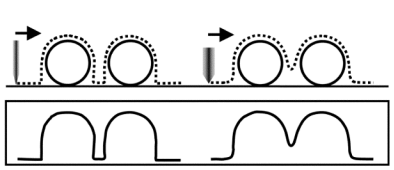

**Figure 3.** Tip shape and in-plane resolution.

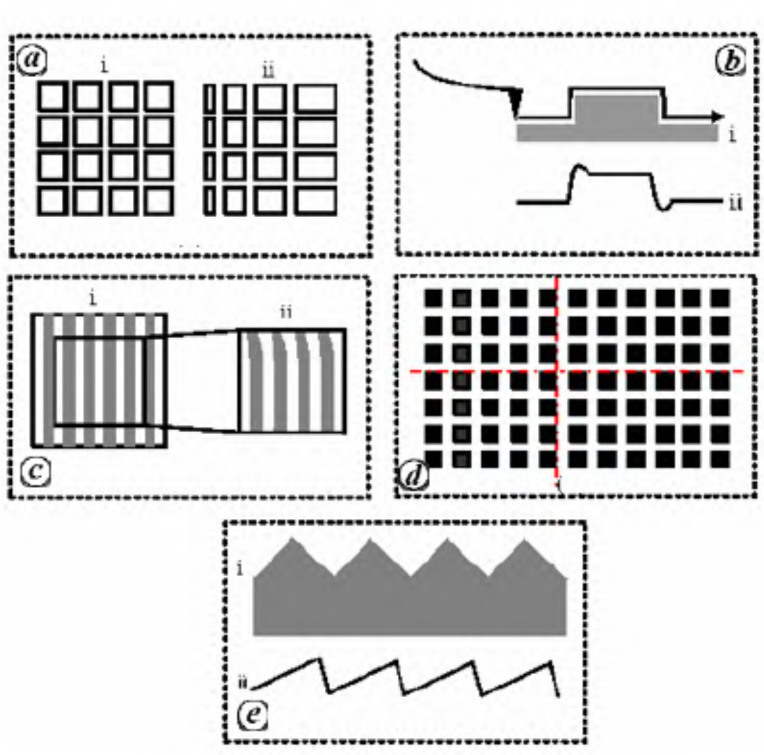


**Figure 4.** Artifacts in AFM image. ***a***, *X*–*Y* nonlinearity; ***b***, *z*-edge overshoot; ***c***, Drift, and ***d***, Angular distortion and ***e***, *z*-angular distortion (see text for details).

Staveley) having outer diameter 12.5 mm and length 75 mm. This piezo tube has four nickel electrodes (4 × 90, slots) on the outer diameter and one electrode in the inner diameter. It can achieve a maximum *Z*-displacement up to 5 μm and *X*–*Y* displacement up to 30 μm. The piezo tube is mounted in a cylindrical aluminum housing for approach mechanism. A teflon ring is affixed at the free end of the piezo tube on which a magnetic chuck is fixed with adhesive. The sample to be imaged is mounted on the sample holder with the help of double-sided tape and thereafter sample holder is placed on the magnetic chuck. The laser spot is focused on the back of the polished cantilever through a laser diode operating at 670 nm wavelength and 1.2 mW power (Melles Griot). *X*–*Y* positioning screws are provided for adjustment. The reflected laser beam from the back of the cantilever is positioned on the active area of a 2D PSD, through a reflecting mirror. The PSD (Pacific Silicon Sensor) has a quadratic photodiode array with current-to-voltage amplifiers that provide bottom-minus-top and left-minus-right difference signals. It also provides a signal that is the sum of all four-quadrant diode signals. The difference signals are voltage analogues of light intensity sensed by the pairs of photodiode elements in the array. The sample is brought near the tip by moving the sample up (i.e. the piezo tube on which the sample is placed) with a motorized micrometer (DC motor mike actuator, Oriel Instruments) having 0.05 μm resolution. Coarse and fine approach is achieved by changing the motor drive signals and thus the speed of the micrometer. An electronic controller is used to control the motion of an object with respect to another object, e.g. tip with the sample surface. Feedback control is achieved using analogue proportional integral controller, wherein a reference force is set through the computer. The signal obtained from the PSD, after conversion and necessary amplification, is compared with the reference force. When the signal obtained does not match the set reference signal, a correction signal is derived and applied to the *z*-segment of piezoscanner moving the sample up or down in accordance with the resultant signal magnitude and polarity, through this control mechanism. The output of feedback is also given to the computer for recording the applied correction. When the electronic feedback control is switched on, the scanning piezo tube (which moves the sample up and down) can respond to any changes in force, which alter the tip–sample separation to restore the force to a predetermined level. This constant force mode operation enables us to obtain the topographical image of the sample.

Data acquisition is performed by acquiring and storing the data from the feedback control loop. In the constant force mode of scanning, the system stores the successive data values used to correct the tip position in relation with applied *X*–*Y* coordinates. A personal computer (P-IV), having data acquisition and analogue output cards PCI-6052, PCI-6733 (NI), has been used to acquire and process image and force curve data signals, and to generate and control the scanning movements of the piezo scanner. Tip–sample approach mechanism signal is also generated through PCI-6733. All settings (e.g. resolution, scan range, delay, scan gain, etc.) are done before beginning the scanning. Data processing is done to generate 2D and 3D display/images along with a host of program features, e.g. scanning at different angles, plane correction, line correction, image selection, thumbnail view, etc. The software has been developed in Visual Basic. Further details on the instrumentation can be found in Kaul *et al.*[11].

As the tip of the AFM cantilever follows the contour of the surface, it experiences an attractive and/or a repulsive force for the tip–surface distance in nanometre or micrometre range. By monitoring the motion of the probe, a three-dimensional image of the surface can be constructed. Data are usually displayed as a colour mapping for height, e.g. black for low features and white for high features. The line-profile analysis of the image displays the vertical and horizontal dimensions of the surface features along the chosen scan line.

For measurements in vacuum, the AFM is kept in a glass chamber with stainless steel collar (Figure 5 *b*), with the chamber being connected to a rotary pump.

## Calibration and measurement of surface topology

The first step after installation of the instrument is its calibration. To calibrate our instrument, we measured surface topology of a standard grating set (NT-MDT, Europe) – TGZ1, TGZ2, TGZ3, TGX1, TGG1 and TGT1. The surface images are taken for 15 μm × 15 μm scan range (Figure 6). Along with a part of 2D image (1st column, Figure 6), we have also shown the three-dimensional reconstruction (second column, Figure 6) from the multiple single-line profiles for each grating. The 3D image can be rotated for better surface visualization. The line-profile of the image along one arbitrarily chosen scan line is also shown in Figure 6 (third column). The height and period of the gratings are estimated from line-profile analysis (Figure 6) and compared with standard values (Table 1). The tabulated values of the above parameters are the average of several measured data taken along different scan lines.

*TGZ grating series:* Calibration gratings of the TGZ series are one-dimensional, fabricated for *z*-axis calibration of the scanning probe microscope (SPM). The height and period of the gratings measured by us are within 2% of their specified values.

*TGG triangular grating:* The calibration grating TGG1 is a one-dimensional array of triangular steps in the *X* or *Y* direction and has precise angular size. In addition to calibration of the SPM in the *X* and *Y*

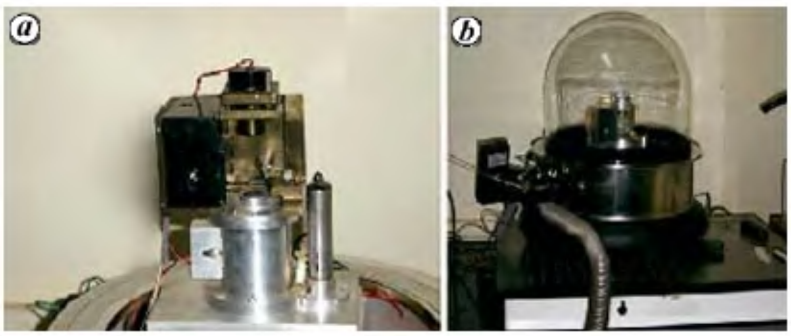


**Figure 5.** Photograph of the AFM designed by us (***a***) and AFM in vacuum bell jar (***b***).

**Table 1.** Calibration of the AFM using standard calibration grating set

| Model grating | Measured | | | | Standard | | | |
|---|---|---|---|---|---|---|---|---|
| | Period (μm) | Height (nm) | Width (μm) | Diagonal period (μm) | Period (μm) | Height (nm) | Width (μm) | Diagonal period (μm) |
| TGZ1 | 3.0 ± 0.04 | 23 ± 0.5 | – | – | 3.0 ± 0.01 | 23 ± 1 | – | – |
| TGZ2 | 3.1 ± 0.04 | 115 ± 1.5 | – | – | 3.0 ± 0.01 | 112 ± 2 | – | – |
| TGZ3 | 3.0 ± 0.05 | 546 ± 2 | – | – | 3.0 ± 0.01 | 545 ± 2 | – | – |
| TGX1 | 3.0 ± 0.04 | 580 ± 1.5 | 1.35 ± 0.04 | – | 3.0 ± 0.05 | 600 | 1.2 | – |
| TGG1 | 2.9 ± 0.03 | 1471 ± 4 | – | – | 3.0 ± 0.01 | 1500 ± 1 | – | – |
| TGT1 | 2.9 ± 0.03 | 584 ± 6 | – | 2.1 ± 0.04 | 3.0 ± 0.05 | 300–700 | – | 2.1 |

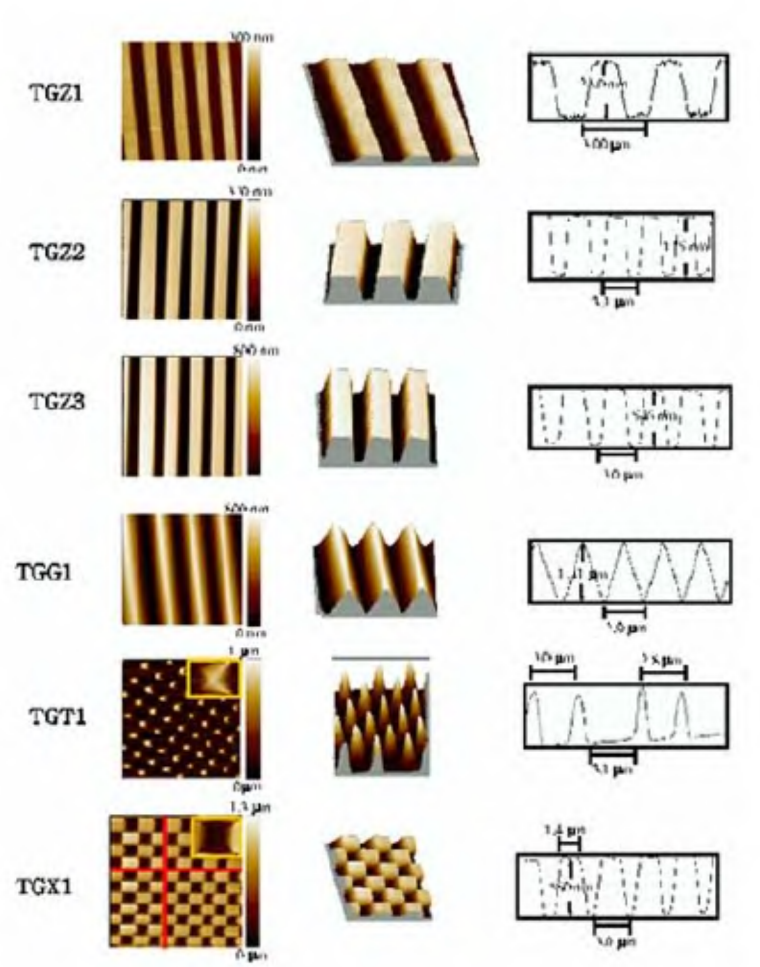


**Figure 6.** Two-dimensional image, 3D reconstruction from line scan and line profile for different calibration gratings. (Inset in the 2D image of TGT1 and TGX1) Image of one unit.

directions, this grating can also be used to check the nonlinearity and angular distortion introduced by the scanner. The undistorted image and symmetric line profile of the triangular grating structure indicates that the scanner of our AFM is corrected for *X*–*Y* nonlinearity and *Z*-angle distortion. Using line-profile analysis and the present software, we could measure the height and period of the grating with reasonable accuracy (Table 1). However, we could not measure the edge angle. Currently, our instrument is not calibrated for angular measurements.

*TGT tip grating:* This calibration grating is an array of sharp tips. It is used for 3D visualization of scanning tips and also for the determination of aspect ratio and radius of curvature of the tip. We could measure the period along the axis and also along the diagonal of the grating (Table 1). However, we could not estimate the tip angle and tip radius of curvature with high accuracy. A scanner with a short scan-range is required for such measurements.

*TGX square grating:* The calibration grating TGX1 is a chessboard-like array of square pillars with sharp undercut edge (with edge curvature less than 10 nm). Along with the lateral calibration of the SPM scanner, this grating can be used to detect the effect of lateral nonlinearity, hysteresis and creep. Two orthogonal vertical lines (red, dotted) indicate reasonable lateral linearity of the scanner (Figure 6). We did not observe the effect of creep in the image. However, the artifact which appears due to hysteresis of the scanner is clear from the *z*-edge overshoot in the line-scan.

*Imaging of gold clusters and germanium dots:* A surface image of gold clusters on Si wafer grown by thermal evaporation technique is shown in Figure 7 *a*. The average height of the gold clusters has been estimated to be 20 nm. The 3D image of germanium quantum dots grown on Si wafer using the sputtering technique is shown in Figure 7 *b*. The average height of the dot is measured to be 120 nm.

## Force measurements

After calibrating the microscope for imaging, we investigate the capability of the instrument in direct force measurements.

The operation of an AFM is based on sensing of spatial variation of the local force fields by measuring the deflection of a micrometre-sized cantilever as it is brought vertically towards a surface. In addition to the gravitational force, other force fields which contribute in force measurement are known to be electromagnetic in nature (electrostatic, magnetostatic and van der Waals). When the tip and sample are in close proximity to each other, the van der Waals interaction is expected to be dominating for a clean, uncharged and nonmagnetic system. The long-range interactions creep in as the separation between them becomes relatively large.

Experimentally, a voltage applied to the electrodes in the *z*-axis of the scanner causes it to expand and then contract in the vertical direction, generating a relative motion between the cantilever and the sample. This determines the separation between the tip and the sample. During force measurement, the deflection of the free end of the cantilever, due to local fields, is measured and plotted at many points, as the *z*-axis of the scanner extends towards the cantilever and then retracts. By controlling the amplitude and frequency of the applied voltage, one can vary the distance that the PZT travels during the force measurement. A typical force curve (force-versus-separation between tip and sample) obtained from our AFM is shown in Figure 8. At maximum resolution, the plate is moved towards the tip of the cantilever in steps of 0.15 nm and the corresponding PSD signal measured at each step (approach curve). Region 1 in Figure 8 corresponds to attractive force between the tip and the sample. For a relatively large separation between the tip and the sample, the PSD signal has two components: (i) a linear part due to increased coupling of the scattered light of the laser into the detector as the sample surface approaches the tip[12] and (ii) a long-range electrostatic force between the tip and the sample, if there is a finite potential drop at the plate/cantilever. For a close separation between the two, the van der Waals force between the tip and the sample dominates. Region 2 in Figure 8 corresponds to the flexing of the cantilever, resulting from the continuous extension of the PZT after contact between the tip and the sample. The zero separation corresponds to the relative point of contact of the tip and the sample. It does not take into account the roughness of the plate surface. In general, an AFM records the photodiode signal in volts, which is then converted to force unit assuming Hooke's law to be valid in Region 2. If $m$ is the slope of Region 2 and $V$ the photodiode signal at any point on the force curve, the following expression

$$F = V \times \frac{1}{m} \times k, \tag{1}$$

converts the signal to force units. Here $k$ is the force constant of the cantilever. With a force sensitivity of the order of few piconewtons, the AFM is an ideal tool for probing the fundamental interactions which exist in nature.

We have measured the spatial dependence of the force field between two objects. The analytical techniques, followed in order to understand the data obtained, are taken from the literature; some of which we will refer to in the corresponding subsections. It may be noted that one can view the discussions to follow as a calibration method for force measurements, which in turn also checks the reliability of the instrument. Now we discuss two different cases: (A) Force between gold-coated cantilever tip and a flat plate, and (B) Force between a sphere and a flat plate. The experiments in (A) and (B) can help us understand the nature of electromagnetic interactions under different experimental conditions and sample geometries.

### *A. Force between AFM tip and flat plate*

The van der Waals force between two surfaces arises due to the interaction of instantaneous oscillating dipoles in these two materials. Between two atoms, the force varies with their separation ($z$) as $z^{-6}$. However, the macroscopic geometries of extended neutral bodies have to be considered in order to understand the contribution from van der Waals interactions in force measurements. This interaction influences many macroscopic phenomena like surface tension, adhesion, colloidal stability, etc. There are many articles available in the literature, where the force–distance curve obtained from the AFM has been modelled by taking the tip of the probe as a sphere or a plane surface. However, these models fail to describe the experimental observations[13–16]. Argento and

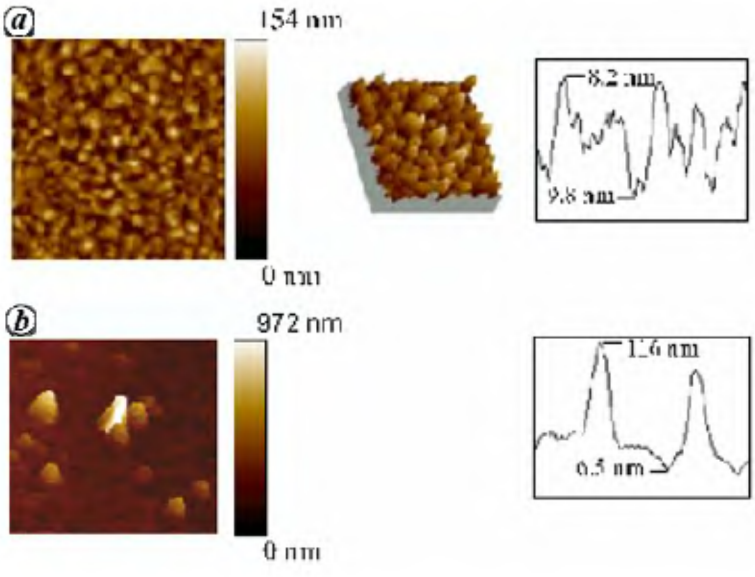


**Figure 7.** AFM image and line profile analysis: (***a***) Gold clusters and (***b***) Ge dots.

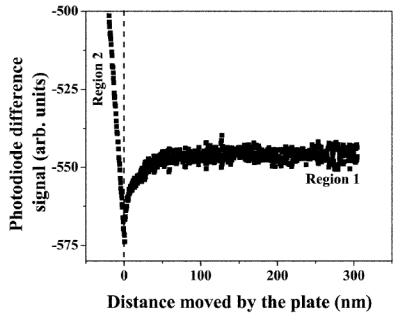


**Figure 8.** A typical force vs distance (moved by the plate) curve as obtained in our AFM.

French developed a parametric model using surface integration method to compute the force–distance relation obtained in an AFM[17]. Their model assumes the tip of the cantilever to be a cylinder followed by a conical section and a spherical cap (Figure 9). The model is completely defined by two parameters: the tip radius $R$ and the cone angle $\gamma$. According to this parametric tip-model, the total van der Waals force on the probe due to a flat surface is[17]:

$$F_{\mathrm{v}}(z) = \frac{\left[\begin{array}{c} AR^2(1-\sin\gamma)\times \\ (R\sin\gamma - z\sin\gamma - R - z)\end{array}\right]}{6z^2(R - z - R\sin\gamma)^2} + \frac{-A\tan\gamma[z\sin\gamma + R\sin\gamma + R\cos(2\gamma)]}{6\cos\gamma(z + R - R\sin\gamma)^2}. \quad (2)$$

The van der Waals interaction can be quantified through the Hamaker constant, $A$, for a pair of materials. The first term corresponds to the contribution of the spherical cap and the second term originates from the cone component of the tip.

We have used commercial silicon nitride cantilevers (model no. MLCT-AUNM, Veeco) for the force measurements. Out of six types of cantilevers available in each probe, we used the one with force constant 0.5 N/m. The cantilevers were coated with a thin layer of gold. Because of the thin coating, the force constant of the coated cantilever is assumed to be same as that of the uncoated one. A 1 sq. cm polished silicon (Si) wafer was coated with gold (99.99%) by thermal evaporation technique and used as a gold-coated plate for the force measurements. The plate was grounded with the AFM. To measure the force between the cantilever tip and surface of Si, a polished Si wafer (100) was cleaned in acetone in a ultrasonic cleaner and then dipped in 1% HF for 2 min. The wafer was then thoroughly washed in deionized water followed by quick drying by an air-blower. The Si wafer showed finite resistance after cleaning. It was then grounded with the AFM for force measurements. In order to minimize the contamination of the surface and to perform measurements where the aerodynamic effects due to the oscillating cantilever are less, we measured the force at 0.4 mbar.

The force–distance curve between the cantilever tip and gold surface, measured using our AFM, is shown in Figure 10 *a*. The nonlinear least square fit to the datapoints with

$$F = F_0 + F_{\mathrm{V}}(z + z_0), \quad (3)$$

keeping $F_0$ (the DC offset to the force curve) and $A$ as free fitting parameters, is shown by the green line in Figure 10 *a*. $z_0$ is the absolute separation between tip and the plate at contact. It is not zero due to finite roughness of the plate. The value of $z_0$ has been constrained to 29.6 ± 0.2 nm (the mean roughness of the plate, as measured by our AFM) to obtain the fit. We constrained the value of $R$ = 20 ± 4 nm and $\gamma$ = 0.665 ± 0.05 (the available specifications for the cantilever are $R$ = 20 nm, $\gamma$ = 0.615). Equation (3) fits the experimental datapoints for a small range with the value of $A$ = 4 zJ. It is clear that a different force starts to dominate the force curve for $z$ > 30 nm. The nature of the onset of this interaction for a relatively large separation between the tip and the sample is given by Argento and French[17]. The authors did not quantify this interaction between the tip and the sample, though the effect has been demonstrated. In addition, the Hamaker constant for a gold-coated AFM probe on a flat surface was obtained by Rabinovich and Churaev[18] to be in the range 90–300 zJ – an order of magnitude different from 4 zJ as obtained from the above nonlinear curve-fitting. We have mentioned before that in the absence of an electrostatic interaction, a force due to coupling of scattered light from the sample to the detector (as the sample is approached) contributes as a linear signal. The net fitted curve with $F(z + z_0) = C + B \times (z + z_0) + F_{\mathrm{V}}(z + z_0)$, keeping $B$, $C$ and $A$ as free fitting parameters, is shown by the red line in Figure 10 *a*. The value of $A$ has been obtained as 117 zJ, which is within the range of its expected values.

Similar analysis has been carried out for the force–distance curve for a gold-coated cantilever tip and polished silicon wafer (Figure 10 *b*). The datapoints are fitted with $F_0 + F_{\mathrm{V}}$ (green line, Figure 10 *b*) and also by a combined function $F(z) = C + B \times (z + z_0) + F_{\mathrm{V}}(z + z_0)$ (red line, Figure 10 *b*). We kept $C$, $B$, $z_0$ and $A$ as free fitting parameters. The values of $R$ and $\gamma$ have been kept fixed to those obtained from the above analysis. The red line corresponds to the value of $z_0$ = 26.7 ± 0.1 nm and $A$ = 280 ± 20 zJ. As in this case the tip of the cantilever could approach the Si surface closer than in the case of the gold surface, onset of this force could be clearly seen through many datapoints.

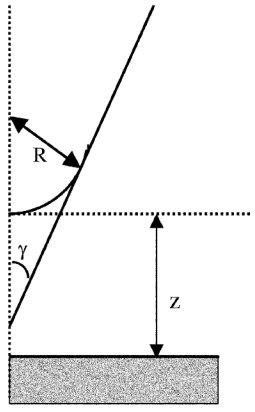


**Figure 9.** Parametric tip model. $R$ is the tip radius and $\gamma$ is the cone angle. $z$ is the probe–sample separation distance.

## B. Force between sphere and flat plate

*Force between gold-coated sphere and plate:* To measure the force curve in plate–

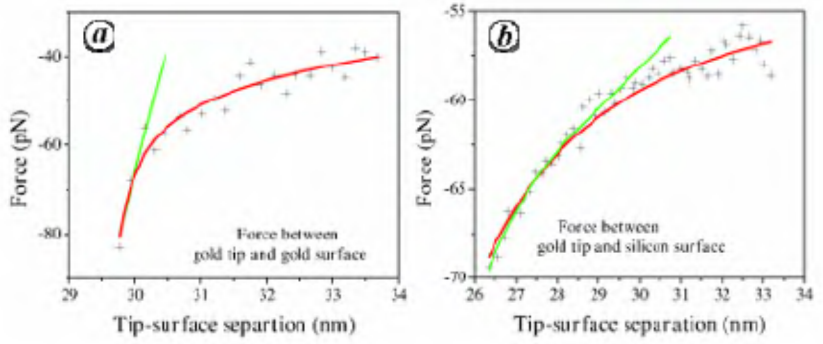


**Figure 10.** Force–distance curve for (***a***) gold-coated AFM tip and gold plate and (***b***) gold-coated AFM tip and polished Si wafer.

sphere geometry, we mounted a 200 ± 4 μm polystyrene sphere (Duke Scientific Corp., CA, USA) on a 350 μm long gold-coated cantilever (NT-MDT-Europe) of force constant 0.01 N/m by silver epoxy. A photograph of the cantilever–sphere assembly is shown in Figure 11. The mount was then coated with gold on both sides. The radius of the mounted polystyrene sphere was measured to be 205 μm. As before, a one sq. cm polished, silicon wafer coated with gold was used as a plate. The plate was grounded together with the AFM and the experiment carried out at 0.35 mbar.

Estimation of residual potential on the sphere: The residual potential on the cantilever–sphere assembly arises due to difference in materials, used to ground the sphere. We calibrated the cantilever–sphere assembly using electrostatic measurements[19]. The electrostatic force between a sphere of radius $R$ at a distance $z$ from the plate is given by[20]

$$F_{\mathrm{E}} = 2\pi\varepsilon_0 (V_1 - V_2)^2 \times \sum_{n=1}^{\infty} \mathrm{csch}\, n\alpha (\coth\alpha - n\coth n\alpha), \tag{4}$$

where $V_1$ is the applied voltage on the plate and $V_2$ the residual potential on the grounded sphere. Here, $\alpha = \cosh^{-1}(1 + \frac{z}{R})$. For $R >> z$, the above equation reduces to

$$F_{\mathrm{E}} = \frac{-\pi\varepsilon R^2 (V_1 - V_2)^2}{z^2}. \tag{5}$$

We measured the electrostatic force between the sphere and the plate by applying ±1.6, ±2.3 and ±3.2 V to the latter ($V_1$). The force curves for the plate voltage ±1.6 V are shown in Figure 12 *a*. Using eq. (5) and from the ratio of measured photodiode signals for each pair at a far distance (>500 nm), the residual voltage $V_2$ on the sphere has been estimated to be 12 mV (on average).

Calibration of the cantilever–sphere assembly: The force constant of a commercial cantilever is known. However, it is modified when we mount a sphere at the tip of the cantilever. The force and the corresponding cantilever deflection (Δz) are related by Hooke's law, $F = k\Delta z$, where $k$ is the force constant of the cantilever. Using Hooke's law and the measured force from eq. (5), the modified force constant of the cantilever has been estimated to be 0.035 N/m (on average).

The force–distance curve measured between a gold-coated sphere and a gold-coated plate (grounded with AFM) is shown in Figure 12 *b*. Due to finite roughness of the coating on both the sphere and the plate, we could not bring the two surfaces closer than 50 nm. Thus, the study on van der Waals interaction could not be carried out in this case. We have fitted the datapoints with $F = F_0 + F_{\mathrm{E}}(z + z_0)$, keeping only $F_0$ and $z_0$ as free fitting parameters (red line, Figure 12 *a*).

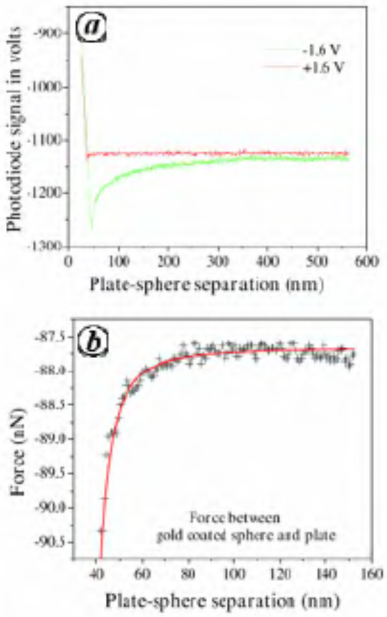


**Figure 12.** ***a***, Typical force–distance curves between polystyrene sphere and gold-ended plate for applied voltage of ±1.6 V to the plate. ***b***, Measured electrostatic force between gold-coated sphere and a gold-coated plate grounded to AFM.

We would like to point out that $R$ and $V_2$ have been measured independently, and kept fixed in fitting procedure. Note that $V_1 = 0$ as the plate is grounded to AFM.

*Force between a polystyrene sphere and a gold plate:* To measure the force curve for a polystyrene sphere and a gold plate, we mounted a 200 μm sphere on the cantilever as before. The gold plate was grounded with AFM. The measurement was carried out at 0.4 mbar.

Patch charge effect: When the polystyrene sphere comes in contact with the plate, a region becomes locally charged[21]. Upon withdrawal, charge remains accumulated in an effective spherical region (Figure 13 *a*) of radius[22]

$$R_{\mathrm{eff}} = \left(\frac{6\pi R^2 W}{K}\right)^{1/3}, \tag{6}$$

where $W$ is the work of adhesion, given by

$$W = \gamma_{\mathrm{ps}} + \gamma_{\mathrm{Au}} - 2\sqrt{\gamma_{\mathrm{ps}}\gamma_{\mathrm{Au}}}. \tag{7}$$

We have taken the surface free energy of polystyrene ($\gamma_{\mathrm{ps}}$)[23] to be 0.033 N/m and that of gold ($\gamma_{\mathrm{Au}}$)[24] to be 1.4 N/m. In eq. (6), $K$ is given by

$$K = \frac{4}{3}\left(\frac{1-\nu_{\mathrm{ps}}^2}{E_{\mathrm{ps}}} + \frac{1-\nu_{\mathrm{Au}}^2}{E_{\mathrm{Au}}}\right)^{-1}. \tag{8}$$

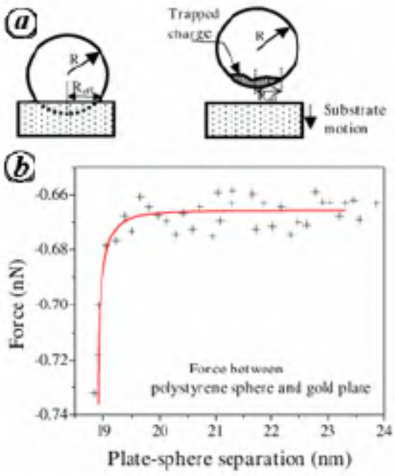


**Figure 13.** ***a***, Patch charge and effective radius of the polystyrene sphere. ***b***, Force–distance curve for polystyrene sphere and gold plate.

**Figure 11.** CCD image of cantilever–sphere assembly and its reflection on metal surface. We estimated the size of the sphere from microscopic 2D image, shown in the inset.

Here $\nu_{ps}$ and $\nu_{Au}$ are the Poisson ratios of polystyrene and gold respectively. $E_{ps}$ and $E_{Au}$ are the Young's moduli of polystyrene and gold respectively. We have taken $\nu_{ps} = 0.35$, $\nu_{Au} = 0.44$, $E_{ps} = 3$ Gpa and $E_{Au} = 78$ GPa. Using eqs (6–8) and the above values for the constants, $R_{eff}$ has been estimated to be 3.39 μm for the measured value of $R = 200$ μm.

Calibration of the cantilever with a sphere: It was not possible for us to measure the residual charge on the uncoated sphere by electrostatic measurements (as discussed earlier). Each time the sphere stuck to the free plate (not grounded) due to the large cohesive force between the two. We have assumed the force constant of the uncoated cantilever–sphere assembly to be the same ($k$ = 0.035 N/m) as it was for the coated one. Note that the increase in force constant of the cantilever with the sphere due to coating is comparatively less than that due to the sphere of 200 μm alone. It may be possible to carry out electrostatic measurements with an uncoated sphere under better vacuum conditions. In that case, $R_{eff}$ needs to be used in place of $R$ in eq. (5).

Figure 13 *b* shows the force-separation curve for a polystyrene sphere and a gold plate as recorded using our AFM. The van der Waals force between a sphere and a neutral surface is given by[25]

$$F_V^S = -\frac{2AR^3}{3z^2(z+2R)^2}, \quad (9)$$

where $A$ is the Hamaker constant, and $z$ the separation between the sphere and the surface.

For $z << R$, eq. (9) is reduced to

$$F_V^S \cong -\frac{AR}{6z^2}. \quad (10)$$

We fit the experimental datapoints with $F = F_0 + F_V^S(z + z_0)$ with measured value of $R$, keeping only $F_0$ as the free fitting parameter. The value of $z_0$ has been chosen to be $18.7 \pm 0.01$ nm (the mean roughness of gold plate we used). The best fit obtained is shown by the red line in Figure 13 *b*. Here, we have used the known value of $A = 112$ zJ (for polystyrene and gold)[26] in eq. (10). Within our experimental accuracy, we find that for this particular configuration, the change in the nature of interaction does not set in appreciably within the $z$-range of our experiment. Gady *et al.*[21] identified the electrostatic and van der Waals interaction in micrometre size polystyrene sphere and flat plate by force gradient measurement. The authors have demonstrated the transition above 30 nm. Here, we have not shown the transition region, as we could not measure the residual voltage on the sphere independently.

## Summary

Understanding the various physical phenomena at the nanoscale, is one of the major interests of the 21st century. An AFM can be used as a tool for this purpose. We have described the design and fabrication of a home-built AFM, which can operate under low vacuum. We have discussed the details of the instrumentation. To establish the performance of our instrument for studying surface topology of materials, we calibrated the instrument with different standard grating structures. These standards are chosen so that we could test the performance of the instrument against various artificial effects.

The principle of an AFM is based on the force between two extended bodies, when their separation is in the nanometre scale. We have measured the force between the cantilever tip and a flat plate as also between a sphere and a flat plate. The van der Waals and Coulombic interactions between two surfaces, in the above cases, have been analysed to check the reliablity of the instrument for direct force measurements. Such a study may help one to understand the basic forces in nature.

With our present set-up, we could not measure forces below 0.4 mbar. We believe that this may not be a limitation; rather a better vacuum unit needs to be designed for high vacuum measurements.


1. Binnig, G., Quate, C. F. and Gerber, Ch., *Phys. Rev. Lett.*, 1986, **56**, 930–933.
2. Binnig, G., Rohrer, H., Gerber, Ch. and Weibel, E., *Phys. Rev. Lett.*, 1982, **49**, 57–61.
3. Binnig, G., Rohrer, H., Gerber, Ch. and Weibel, E., *Phys. Rev. Lett.*, 1983, **50**, 120–123.
4. Guenther, K. H., Wierer, P. G. and Bennett, J. M., *Appl. Opt.*, 1984, **23**, 3820–3836.
5. Thalhammer, S. and Heckl, W. M., In 4th IEEE Conference on Nanotechnology, 2004, pp. 577–579.
6. Hankea, A., Boeck, T. and and Gerlitzke, A.-K., *Appl. Phys. Lett.*, 2006, **88**, 173106-1–173106-3.
7. Putman, C. A. J., De Grooth, B. G., Van Hulst, N. F. and Greve, J., *J. Appl. Phys.*, 1992, **72**, 6–12.
8. Meyer, G. and Amer, N. M., *Appl. Phys. Lett.*, 1988, **53**, 1045–1047.
9. Meyer, G. and Amer, N. M., *Appl. Phys. Lett.*, 1990, **57**, 2089–2091.
10. Brar, L. K., Paranjape, M., Guha, A. and Raychaudhuri, A. K., *Curr. Sci.*, 2002, **83**, 1197–1199.
11. Kaul, A. D., Singh, N., Sonkusare, A., Kumar, P. and Wadhwa, S. S., *Curr. Sci.*, 1997, **73**, 738–743.
12. Mohideen, U. and Roy, A., *Phys. Rev. Lett.*, 1998, **81**, 4549–4552.
13. Hartmann, U., *J. Vac. Sci. Technol.*, 1991, **9**, 465–469.
14. Senden, T. J., Drummond, C. J. and Kekicheff, P., *Langmuir*, 1994, **10**, 358–362.
15. Biggs, S. and Mulvaney, P., *J. Chem. Phys.*, 1994, **100**, 8501–8505.
16. Ducker, W. A. and Clarke, D. R., *Colloids Surf.*, 1994, **94**, 275–292.
17. Argento, C. and French, R. H., *J. Appl. Phys.*, 1996, **80**, 6081–6090.
18. Rabinovich, Y. I. and Churaev, N. V., *Russ. J. Phys. Chem.*, 1990, **52**, 256–262.
19. Roy, A., Lin, C.-Y. and Mohideen, U., *Phys. Rev. D*, 1999, **60**, 111101-1–111101-5.
20. Smythe, W. R., *Electrostatics and Electrodynamics*, McGraw Hill, New York, 1950.
21. Gady, B., Schleef, D., Reifenberger, R., Rimai, D and DeMejo, L. P., *Phys. Rev. B*, 1996, **53**, 8065–8070.
22. Johnson, K. L., Kendall, K. and Roberts, A. D., *Proc. R. Soc. London, Ser. A*, 1971, **324**, 301.
23. Gesche, R., Kovacs, R. and Scherer, J., *Surf. Coat. Technol.*, 2005, **200**, 544–547.
24. Kumikov, V. K. and Khokonov, Kh. B., *J. Appl. Phys.*, 1983, **54**, 1346–1350.
25. Hamaker, H. C., *Physica*, 1937, **4**, 1058–1072.
26. Gady, B. L., Ph D thesis, Purdue University, USA, 1996.


ACKNOWLEDGEMENTS. A.R. thanks DRDO, India for financial support and Dr V. Siddharth for interest and support during the early stages when the project was being planned. A.S. thanks CSIR, New Delhi for Senior Research Fellowship.

Received 20 March 2007; revised accepted 22 August 2007

*Achintya Singha and Anushree Roy* are in the Department of Physics, Indian Institute of Technology, Kharagpur 721 302, India, and Anil Sonkusare, Pradeep Kumar and A. D. Kaul are in the MSD Division, Centre for Scientific Instruments Organization, Chandigarh 160 020, India.*

**e-mail: anushree@phy.iitkgp.ernet.in*